Niels Thevs, Rainer Nowotny[1]

Water consumption of industrial hemp (*Cannabis sativa* L.) during dry growing seasons (2018–2022) in NE Germany

Wasserverbrauch von Industriehanf (*Cannabis sativa* L.) während trockener Vegetationsperioden (2018–2022) in Nordostdeutschland

Affiliation
[1]Hanffaser Uckermark, Prenzlau, Germany.

Correspondence
Dr. Niels Thevs, E-Mail: niels.thevs@gmail.com

Abstract

Europe experienced unprecedented droughts during the years 2018, 2019, and 2020. In the course of climate change, it is expected that such drought events will occur more frequently so that agriculture needs to adapt to droughts. Hemp (*Cannabis sativa* L.) has been promoted as an adaptation to water limited conditions. Hemp delivers biomass as a raw material to a variety of different value chains, such as fibers and textiles, house construction, chemicals, or food applications.

Hemp develops a deep root system, which enables it to cover its water demand even during longer dry periods. This may lead to an over exploitation of soil moisture of deeper soil layers or of the groundwater in the long-term. Against this background, this study assessed the water consumption of hemp in Northeastern Germany (region Uckermark) during the growing seasons 2018–2022. The Penman Monteith approach was used to calculate the water consumption, whereby the remote sensing based S-SEBI approach was employed, with Landsat satellite images as input data, to feed crop coefficients into those calculations.

The water consumption of hemp ranged from 310 to 407 mm over the growing seasons 2018–2022, while stem yields were 9 t ha^{-1} (except 2018 with 7.8 t ha^{-1}). This water consumption did exceed the precipitation during the growing seasons, but did not exceed the total precipitation of the given hydrological years so that growing hemp does not constitute an over-exploitation of water. Instead, hemp taps the soil moisture that has infiltrated into the soil during autumn and winter. This makes hemp a crop well suited for an adaptation to a drier, hotter, and more variable climate.

Keywords

biomass, renewable raw material, water consumption, evapotranspiration, climate change adaptation, agriculture

Zusammenfassung

In den Jahren 2018, 2019 und 2020 war Europa von einer extremen Dürre betroffen. Im Zuge des Klimawandels wird davon ausgegangen, dass Dürren häufiger auftreten und extremer ausfallen, so dass die Landwirtschaft sich an Trockenperioden anpassen muss. Der Anbau von Hanf (*Cannabis sativa* L.) wird als eine Möglichkeit der Anpassung an Trockenperioden angesehen. Hanf liefert Biomasse als Rohstoff für eine Reihe von Wertschöpfungsketten, z. B. für Fasern und Textilien, als Baumaterial, Chemikalien oder als Nahrungsmittel.

Hanf bildet ein tiefgehendes Wurzelsystem, durch das die Hanfpflanze ihren Wasserbedarf auch während längerer Trockenphasen aus tieferen Bodenschichten decken kann, was zu einem Entzug der Bodenfeuchte aus dem Unterboden führen kann. Vor diesem Hintergrund wurde in dieser Studie der Wasserverbrauch von Hanf auf Standorten in Nordostdeutschland (Uckermark) in den Jahren 2018–2022 ermittelt. Dafür wurde der Penman-Monteith Ansatz verwendet, wobei die fernerkundungsbasierte Methode S-SEBI, mit Landsat Satellitenbildern als Datengrundlage, eingesetzt wurde, um Crop-Koeffizienten in diese Penman Monteith Berechnungen einzuspeisen.

Der Wasserverbrauch von Hanf lag zwischen 310 mm und 407 mm, jeweils für die Vegetationsperioden 2018–2022 bei Stängelerträgen von 9 t ha^{-1} (außer 2018 mit 7,8 t ha^{-1}). Diese Wasserverbräuche überstiegen die Niederschläge während der jeweiligen Vegetationsperioden, sie überstiegen jedoch nicht die Jahresniederschläge der jeweiligen hydrologischen Jahre. Daher übernutzt Hanf nicht die Bodenfeuchte, sondern Hanf nutzt die Bodenfeuchte, die im Herbst und Winter in den Boden infiltriert war, so dass Hanf dadurch gut an ein trockeneres, wärmeres und variableres Klima angepasst ist.

Stichwörter

Biomasse, nachwachsender Rohstoff, Wasserverbrauch, Evapotranspiration, Anpassung an Klimawandel, Landwirtschaft

Submitted/accepted for publication: 1 March 2023/13 June 2023

Introduction

Europe experienced an unprecedented drought during the years 2018, 2019, and 2020 (Rakovec et al., 2022). Already before 2018, Europe had been hit by a number of dry summers, as in 2003, 2010, and 2015. Droughts are estimated to cause an annual damage of 9 billion EUR across Europe, whereby 39%–60% of all damages hit agriculture (Naumann et al., 2021). Moreover, climate change increased the probability of the occurrence of such drought events (Hari et al., 2020), underlining that agriculture needs to adapt to drier and hotter summers in general and severe drought events in particular. Within Germany, the climate in Eastern Germany is drier and more continental compared to Western Germany so that the drought of 2018–2020 affected a larger share of farmland in East Germany compared to the rest of the country, as highlighted by Amt für Statistik Berlin-Brandenburg (2019).

Hemp (*Cannabis sativa* L.) has been promoted as a crop, which produces marketable harvest under water-limited conditions, as shown by Struik et al. (2000). Lisson & Mendham (1998) measured stem yields of 10 t ha^{-1} and total biomass dry matter yields of 12 t ha^{-1} under rainfed conditions with rainfalls below 300 mm during the growing season. In addition, hemp is a multi-purpose crops, which delivers biomass as a raw material to a variety of different value chains, such as fibers and textiles, house construction, chemicals, or food applications (Amaducci & Gusovius, 2010; Moscariello et al., 2021). Globally, there is an increasing demand for biomass as a raw material for the bio-economy in the course of abandoning fossil raw materials. Hemp biomass can help to address this demand and hence provide new opportunities for rural regions (Ingrao et al., 2018).

Hemp develops a deeper root system than most other crops, such as cereals, which enables it to exploit deeper soil layers or the groundwater to cover its water demand even during longer dry periods (Struik et al., 2000). Thereby, hemp exploits soil moisture, which has been accumulated from the precipitation that has occurred before the onset of the development stage of hemp with its rapid growth (Thevs & Aliev, 2022). This makes hemp a potentially attractive crop under increasingly dry conditions, but also may lead to an over exploitation of soil moisture of deeper soil layers or of the groundwater in the long-term. Against this background, this study aimed at assessing the water consumption of hemp grown for industrial use.

This study uses the term water consumption as a synonym of evapotranspiration, as defined as follows: Activities that divert water from its source; water that is no longer available because it has evaporated, been transpired by plants, incorporated into products or crops, consumed by people or livestock, or otherwise removed from the immediate water environment (https://www.watercalculator.org/footprint/water-use-withdrawal-consumption/).

The Penman-Monteith approach by FAO (Allen et al., 1998) is a standard method to calculate crop evapotranspiration (ET_c), whereby climate data from standard climate stations and so-called crop coefficients (K_c) are taken as input data. Such crop coefficients, which reflect the water consumption of crops with sufficient water and nutrient supply, are available for the major global crops from a number of regions. For hemp, only a limited number of studies provide such K_c values, which all are from drier and warmer climates and different crop development stages compared to the study area of this study (Thevs & Aliev, 2022; Noghabi et al., 2021; Garcia-Tejero et al., 2014; Consentino et al., 2013). Furthermore, all of those studies, except for Thevs & Aliev (2022), measured K_c values under irrigation to ensure sufficient water supply. In this study, it was unknown whether hemp, which was grown without any irrigation, did enjoy sufficient water supply or not. Therefore, the K_c values by other studies were rejected as input data to calculate the water consumption of hemps.

Instead, K_c values were calculated based on actual evapotranspiration (ET_a) derived through the remote sensing based Simplified Surface Energy Balance Index (S-SEBI) after Roerink et al. (2000), Sobrino et al. (2005; 2007), as reviewed by Gowda et al. (2007; 2008). Those K_c values fed into the calculation of the daily crop water consumption after Allen et al. (1998). For clarity, the term ET_a refers to evapotranspiration by crops assessed through remote sensing, while ET_c refers to results from the calculations based on climate data and crop coefficients.

Methods

This study aimed at assessing the water consumption of hemp in the region Uckermark, which is the northeastern part of the Federal State Brandenburg in Northeastern Germany.

In the region Uckermark, the enterprise Hanffaser Uckermark has been contracting farmers to grow industrial hemp, in order to extract fibers for insulation and other construction materials. The five hemp fields (Fig. 1) that were planted to hemp from 2018 until 2022 constituted the core of the study region. Thereby, each year a different field plot was contracted so that for each year a different field was included in this study. Field sizes ranged from 15 ha to 56 ha, while stem yields remained at 9 t ha^{-1} year on year, except for 2018, which yielded 7.8 t ha^{-1}. Fields of winter wheat, which is the major crop in the study region, stands of broad leaf forest, and needle forest, all in the vicinity of the hemp fields, were selected from satellite images, in order to include such areas to validate the mapping of the water consumption. The hemp fields, wheat fields, and forest stands are shown in the map in Figure 1. The climate of the study region is classified as warm and humid continental climate with the main features as listed in Table 1 for the climate station Angermünde.

Hemp was sown around 1st of April in all five years. During the first two weeks after seeding, the seeds germinated and developed their roots and only after those two weeks saplings became visible. During June, hemp grew rapidly, up to several cm per day. Afterwards, beginning of July hemp started to flower, though part of the hemp still flowered during beginning of August. Accordingly, seeds became ripe during July and August, while hemp continued to grow, albeit at a slower speed than during June. All hemp fields were harvested between 15th and 25th August of each year. The stems remained

Table 1. Temperature and precipitation at climate station Angermünde (30-year observation from 1991 until 2021), based on DWD (2022)

Climate feature	Value
Average January temperature [°C]	0.3
Average July temperature [°C]	19.3
Annual precipitation (hydrological year) [mm]	527
Precipitation during growing season (Apr–Oct) [mm]	347

on the fields after harvest for the retting during autumn and winter. The growing season was defined as 1st of April till 31st of October.

To assess the water consumption, as a first step the daily reference evapotranspiration (ET_o), according to FAO (Allen et al., 1998), was calculated from the daily climate data from Angermünde for each day of the growing seasons 2018 to 2021. Climate data for 2022 were not yet available while this manuscript was written. ET_o is calculated into the crop evapotranspiration (ET_c) of a given crop by multiplying ET_o with a crop coefficient (K_c) which is specific by crop and development stage:

$$ET_c = ET_o\, K_c \quad (1)$$

The steps to calculate ET_o are explained in full detail in Allen et al. (1998).

As K_c values from the literature were not used, for each of the remote sensing based ET_a data points a K_c was calculated by ET_a/ET_o. These K_c values were linearly interpolated between ET_a data points and finally allowed to calculate an ET_C based on each day's ET_o (Fig. 2). The daily climate data were downloaded from DWD (2022) for the climate station Angermünde, which was the closest station to the study region.

The ET_a values of each of the ET_a maps were extracted for all the pixels inside each of the designated hemp field, wheat field, and forest stand to calculate the average ET_a of hemp, wheat, broad leaf forest, and needle forest. Thereby, the pixels closer than 100 m to the boundary of the hemp fields, wheat fields, and forest stands were excluded to avoid the impact of mixed pixels. These procedures yielded data points of ET_a for the dates for which satellite images were available

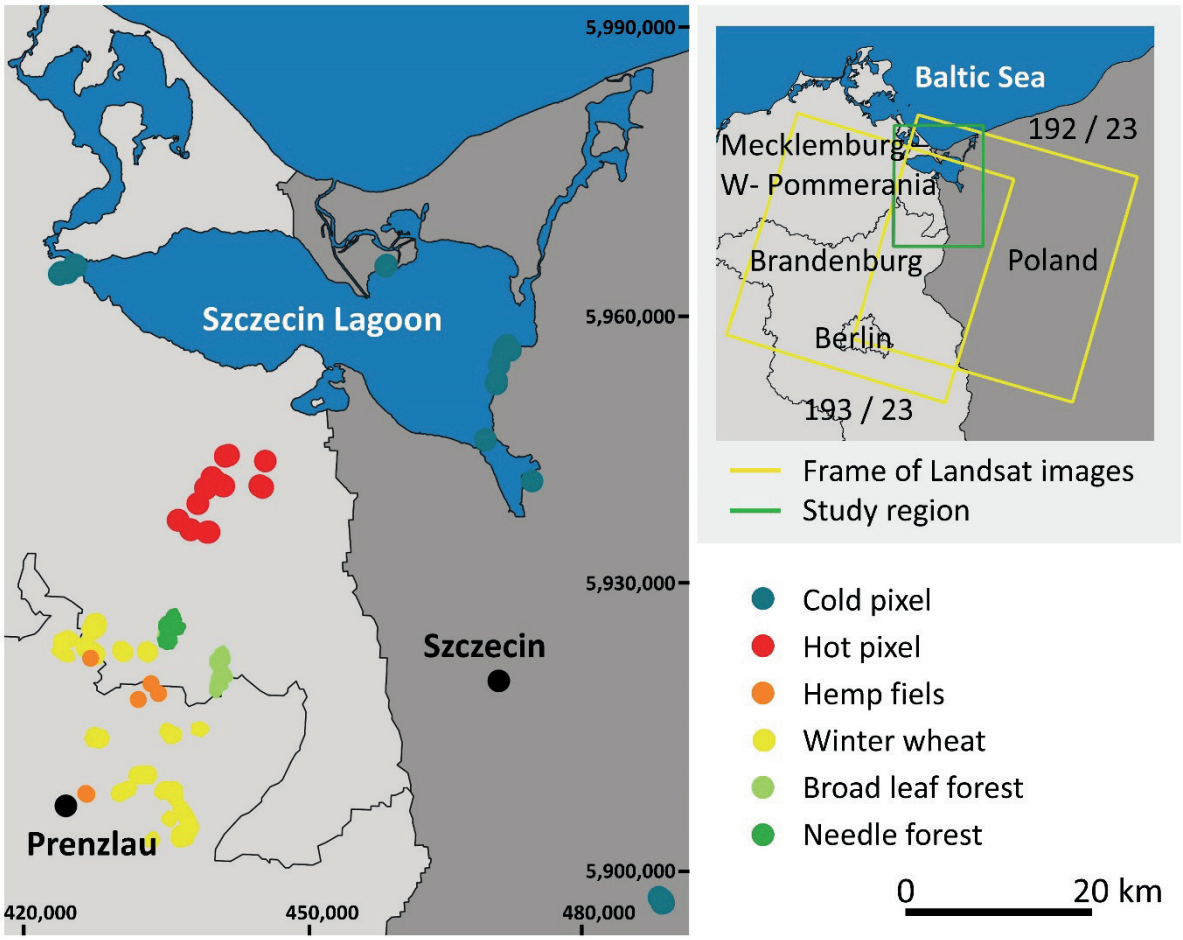

Fig. 1. Map of the study area (detailed map on the left side) and overview map (top right). Coordinates in the detailed map are UTM coordinates (UTM zone 33N). 192/23 and 193/23 indicate the path and row numbering of the two Landsat image frames.

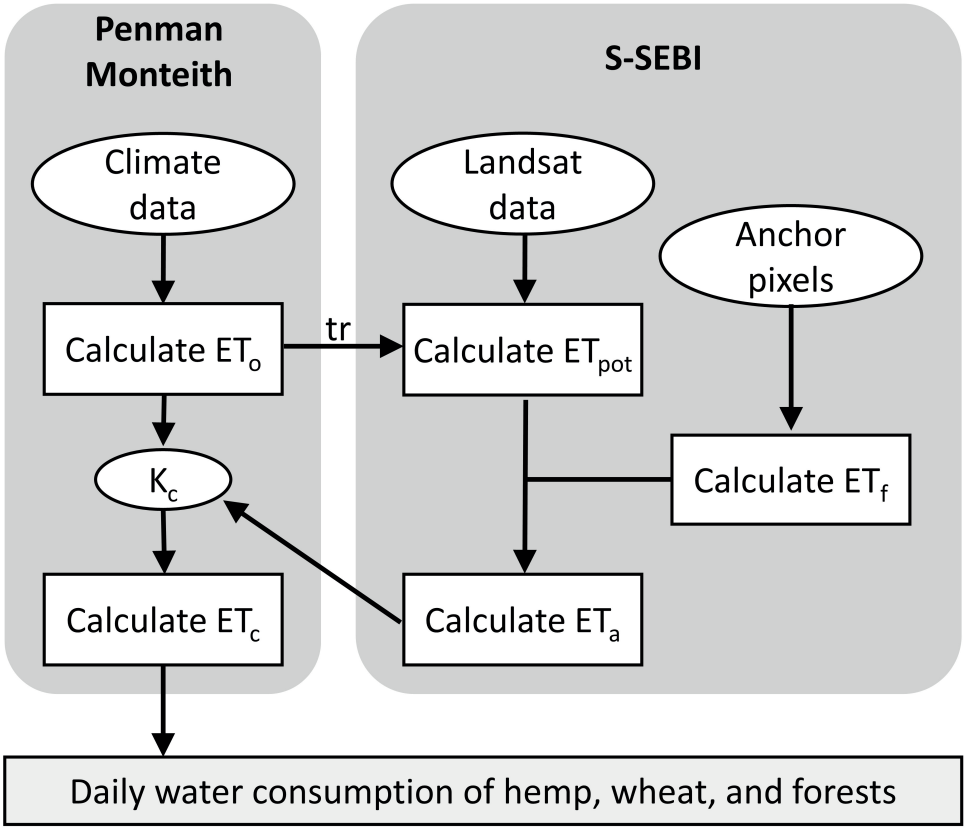

Fig. 2. Flow diagram of the calculation steps of the Penman Monteith and S-SEBI approach. Tr refers to transmissivity.

(Table 2). Wheat, needle forests and broad leaf forests were included, in order to be able to corroborate the results with literature values.

ET_a was assessed through the remote sensing based Simplified Surface Energy Balance Index (S-SEBI) after Roerink et al. (2000), Sobrino et al. (2005; 2007), as reviewed by Gowda et al. (2007; 2008). In this study, Landsat OLI and Landsat ETM + data were used, because their spatial resolution (of 100 m × 100 m in the land surface temperature channel – LST) allowed to map the targeted hemp field plots, while MODIS with its spatial resolution of 1000 m × 1000 m would be too coarse for the purpose of this study.

The S-SEBI is explained in full detail in Hochmuth et al. (2015) and Thevs et al. (2015) for the use of Landsat satellite data and by Thevs et al. (2017) for the use of MODIS data. All handling of the satellite images, other geo-data, and the calculations of water consumption (or evapotranspiration) were done in Q-GIS (version 3.16.7). The Landsat data were converted into radiance and LST further into Kelvin according to USGS (2019).

Remote sensing based approaches that map water consumption use thermal infrared data, such as the LST channel of Landsat (Kustas & Norman, 1996). Those approaches are suited to map water consumption of vegetation for which no solid crop specific data on evapotranspiration are available, such as crop coefficients (Allen et al. 1998), or of vegetation that is water stressed and therefore does not meet the requirements for modelling of evapotranspiration through standard methods as the Penman Monteith approach. Frequently used models, which use thermal infrared data are: Surface Energy Balance Algorithm (SEBAL) developed by Bastiaanssen (1995), Bastiaanssen et al. (1998; 2000; 2002; 2005), Mapping Evapotranspiration with Internalized Calibration (METRIC) after Allen et al. (2005), Surface Energy Balance System (SEBS) according to Su (2002), Simplified Surface Energy Balance (SSEB) by Senay et al. (2007), and Simplified Surface Energy Balance Index (S-SEBI) after Roerink et al. (2000), Sobrino et al. (2005; 2007), and Gowda et al. (2007; 2008). The S-SEBI method does not need additional data, such as climate data, to be able to map the water consumption from a given satellite image, which made it suitable for this study.

In principle, those models solve the surface energy balance for the latent heat flux, which corresponds to the latent heat for evapotranspiration, for each pixel of a given satellite image and calculate the instantaneous evapotranspiration at the satellite overpass time (Bastiaanssen et al., 1998; 2000; Allen et al., 2005). The S-SEBI model calculates the latent heat flux as:

$$LE = \Lambda(R_n - G) \quad (2)$$

with LE, Λ, R_n, and G being the latent heat flux [W m^{-2}], evaporative fraction, net radiation [W m^{-2}], and soil heat flux [W m^{-2}], respectively. Thereby, it is assumed that Λ is constant during the whole day. The daily sum of the soil heat flux is set to zero (Cammalleri et al., 2012).so that equation 1 is simplified for daily values (Sobrino et al., 2005, 2007):

$$LE_d = \Lambda_d R_{nd} \quad (3)$$

LE_d, Λ_d, and R_{nd} refer to daily latent heat flux sum [MJ d^{-1}], daily evaporative fraction, and daily net radiation sum [MJ d^{-1}].

If the daily net radiation (R_{nd}) is converted into evapotranspiration, i.e. potential evapotranspiration (ET_{pot}), ET_a, can be calculated as follows (Sobrino et al., 2005, 2007):

$$ET_a = \Lambda\, ET_{pot} \quad (4)$$

The evaporative fraction (Λ) is the fraction of the ET_{pot}, which is actually realized as ET_a. Thus, over well-watered vegetation, e.g. wetland vegetation, Λ ≈ 1 and $ET_a \approx ET_{pot}$. There, the land surface temperature (LST) is low, because the energy of the incoming radiation is consumed by evapotranspiration. In contrast, Λ and ET_a are zero at places without any vegetation or other moisture. Here, LST is high, because the energy of the incoming radiation goes into the sensible heat flux. Between these two extremes it is assumed that Λ and land surface temperature have a linear relationship (Roerink et al., 2000). So-called cold pixels, where Λ ≈ 1, and hot pixels, where Λ ≈ 0, must be selected from the given satellite image.

The evaporative fraction Λ is calculated as follows:

$$\Lambda = \frac{(T_H - T_x)}{(T_H - T_C)} \quad (5)$$

Thereby T_H, T_C, and T_x refer to the LST at the hot pixel, cold pixel, and pixel, for which Λ is calculated, respectively. The selection of the cold and hot pixels plays a critical role for the resulting ET_a. Cold pixels must show a low LST due to their high evapotranspiration and not due to simply being cold objects, e.g. deeper water bodies. Hot pixels must not exhibit any evapotranspiration and therefore are selected in areas without vegetation. Yet, non-vegetated areas may have a wide range of LST due to their surface characteristics (such as surface color or structure) or geographical location. From that wide range of non-vegetated areas the pixels with the lowest LST must be selected as hot pixels to avoid that Λ will be over-estimated (Waters et al., 2002; Senay et al., 2007). The cold and hot pixels were selected manually for each Landsat image, in order to avoid errors by cloud cover or land cover changes by grazing or changing water levels.

ET_{pot} [mm d^{-1}] is calculated through the following set of formulae (5-8):

$$ET_{pot} = \frac{R_{nd}}{L_{water}\, \rho_{water}} \quad (6)$$

ρ_{water} is the density of water (1005 g l^{-1}), while R_{nd} [MJ m^{-2} d^{-1}] refers to the daily net radiation (cf. equation 7).

L_{water}, the latent heat of vaporization of water [MJ g^{-1}] is calculated by the following equation:

$$L_{water} = 10^6 \left(2500.8 - 2.36\,(LST - 273.15)\right) \quad (7)$$

Thereby, LST is the land surface temperature in Kelvin.

Equation 7 calculates the daily net radiation R_{nd} [MJ m^{-2} d^{-1}]:

$$R_{nd} = R_s\,(1 - \alpha) - 110\, tr \quad (8)$$

α refers to the albedo and tr to the transmissivity. The albedo was calculated from each Landsat image according to Liang (2000).

R_s is the daily solar radiation [MJ m^{-2} d^{-1}] and is calculated as follows:

$$R_s = tr\, R_a \quad (9)$$

tr is the transmissivity. R_a, the extraterrestrial radiation [MJ m^{-2} d^{-1}], was calculated after the respective equations from the Penman-Monteith approach that had been mentioned above to calculate ET_o (Allen et al., 1998). The transmissivity is the fraction of R_a that eventually penetrates the atmosphere down to the earth's surface. For each date of each Landsat image (Table 2) the transmissivity was taken from the respective ET_o calculations.

The water consumption was mapped from Landsat satellite images, Landsat OLI (Landsat 8 and 9) as well as Landsat ETM+ (Landsat 7), path/row 192/23 and 193/23, for the whole study region during the growing seasons from 2018 through 2022. Table 2 lists the Landsat images that were used for this study. On each satellite image, clouds were masked out manually.

The so-called cold pixels were placed manually into wetlands, mainly reed beds, at the coast of the Szczecin Lagoon and Lake Krzekna (appr. 20 km SE of Szczecin City), while the so-called hot pixels were placed into small areas without vegetation, such as intersections of vehicle lanes, on the military training area Torgelow-Eggesin. Thereby, it was made sure that those hot anchor pixels were located close to the surrounding forests and not in the middle of the open tree-less areas.

Results

In all growing seasons, except for 2018, the ET_a values of hemp as derived from the single satellite images remained close to zero for about 20 days after planting (Fig. 3). In 2018, ET_a dropped from 1.3 mm d^{-1} on DOY 92 to 0.1 mm d^{-1} on DOY 108. DOY refers to the n^{th} year of each year. Afterwards, the single ET_a values during all five growing seasons increased steeply and peaked around DOY 180 (which is end of June) with values between 4 mm d^{-1} and 6 mm d^{-1}. From beginning of July until harvest, which takes place end of August (before DOY 240), the ET_a values decrease steadily also across all five growing seasons. The ET_a values from end of August until the end of the growing seasons (31st of Oct) are again close to zero. Only on DOY 261 of 2018 and DOY 253 of 2021, ET_a deviated from this with value of 1 mm d^{-1} and 0.9 mm d^{-1}, respectively. In both cases, there had been rainfall events shortly before.

This course of ET_a over the growing seasons coincided well with the development of hemp as described in the method section. Hence, the highest ET_a values between DOY 150 and 180 match the development stage of hemp, during which it grows rapidly.

The course of ET_a of wheat (winter wheat), broad leaf forest, and needle forest over the growing seasons is also illustrated in Figure 3. Wheat started with ET_a values between 1 mm d^{-1} and 2 mm d^{-1}, climbed up to around 5 mm d^{-1} during May and June, and fell sharply to below 1 mm d^{-1} after its harvest in July. The highest ET_a datapoint with 6.5 mm d^{-1} on DOY 175 of 2019 is two weeks after a five-day long rainy period of 43 mm precipitation in total and two days after a rain fall event of 6.4 mm.

Table 2. Landsat images used for the mapping of the water consumption across the study area

Path	Sensor	Date	DOY	Path	Sensor	Date	DOY
2018				**2020**			
193	LC8	2-Apr-18	92	193	LC8	7-Apr-20	98
193	LC8	18-Apr-18	108	193	LC8	23-Apr-20	114
193	LC8	4-May-18	124	192	LC8	3-Jun-20	155
192	LC8	13-May-18	133	192	ETM+	27-Jun-20	179
193	LC8	20-May-18	140	192	LC8	6-Aug-20	219
192	LC8	29-May-18	149	193	LC8	13-Aug-20	226
192	ETM+	6-Jun-18	157	193	LC8	14-Sep-20	258
192	LC8	16-Jul-18	197	192	LC8	23-Sep-20	267
193	LC8	23-Jul-18	204	**2021**			
192	LC8	1-Aug-18	213	192	LC8	19-Apr-21	109
192	LC8	17-Aug-18	229	192	ETM+	27-Apr-21	117
192	LC8	18-Sep-18	261	193	ETM+	5-Jun-21	156
193	LC8	11-Oct-18	284	192	LC8	10-Sep-21	253
2019				**2022**			
193	LC8	21-Apr-19	111	192	LC8	8-May-22	128
192	LC8	30-Apr-19	120	193	LC9	23-May-22	143
193	LC8	23-May-19	143	192	LC9	17-Jun-22	168
193	LC8	24-Jun-19	175	193	LC8	24-Jun-22	175
193	LC8	26-Jul-19	207	193	ETM+	3-Jul-22	184
193	LC8	27-Aug-19	239	192	LC8	19-Jul-22	200
193	LC8	14-Oct-19	287	193	ETM+	20-Jul-22	201
				193	LC8	3-Aug-22	215
				192	LC9	4-Aug-22	216
				193	LC9	11-Aug-22	223
				192	LC8	12-Aug-22	224
				193	LC8	4-Sep-22	247
				192	LC9	5-Sep-22	248

ET_a of broad leaf and needle forest showed a similar course over the growing seasons, as displayed in Figure 2. During April, ET_a values climbed up from 2 mm d^{-1} and 3 mm d^{-1} in the case of broad leaf forest and needle forest, respectively, to around 6 mm d^{-1}, which were the ET_a values during May and June. After June (DOY 180), ET_a slowly decreased during summer and autumn to fall below 1 mm d^{-1} in October (after DOY 270).

ET_o and ET_c of hemp of those four growing seasons are displayed in Figure 4. This figure also illustrates that the water consumption of hemp remains low during April and sharply increases during May and June which is followed by a sharp decrease after flowering started in July. The sum of those interpolated daily ET_a values revealed that hemp consumed between 312 mm and 407 mm over the growing seasons of 2018 until 2021 (Table 3).

The water consumption of hemp over the growing season of 2022 was 310 mm. When interpolated directly from the ET_a of the satellite images, as done for 2018, 2019, and 2020, the sum of ET_a was 1.2 times higher compared to the interpolation through the K_c values. Accordingly, the result of the interpolation from the satellite images for 2022 was divided by 1.2 to yield the water consumption of hemp for 2022.

The water consumption of hemp and wheat remained below the precipitation of the corresponding hydrological years, which runs from 1st of November of the preceding year till 31st of October of the given year, though exceeded the precipitation during the growing seasons (except in 2021). In contrast, the water consumption of the forests did exceed the precipitation of the corresponding hydrological years, except for 2021 (Table 3).

The K_c values, displayed in Figure 5, behaved roughly as the course of the ET_a over the growing seasons. K_c values remained below 0.1 (except for the beginning of the growing seasons 2018) for 30 days after planting, followed by an increase until 90 days after planting. Accordingly, the initial stage lasted for 30 days and the development stage for 60 days. The mid-stage is short with only 20 days, corresponding to the time during which the K_c values (Fig. 5) as well as ET_a (Fig. 3) remained high. Finally, K_c values decreased until the harvest so that the late stage lasted for the 30 days after the mid-stage. The K_c values that had been calculated for the time

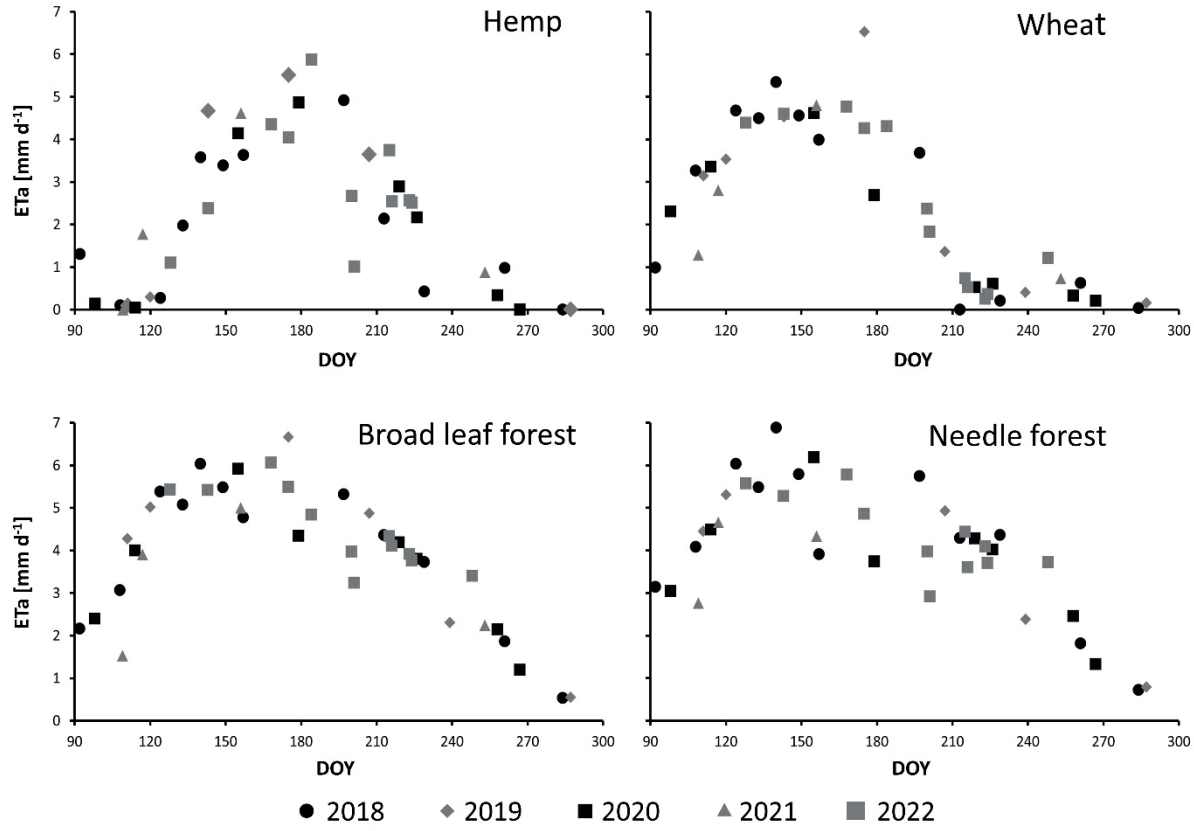

Fig. 3. ET_a data points for hemp, wheat, broad leaf forests, and needle forests over the growing seasons 2018–2022. DOY refers to the n^{th} year of each year.

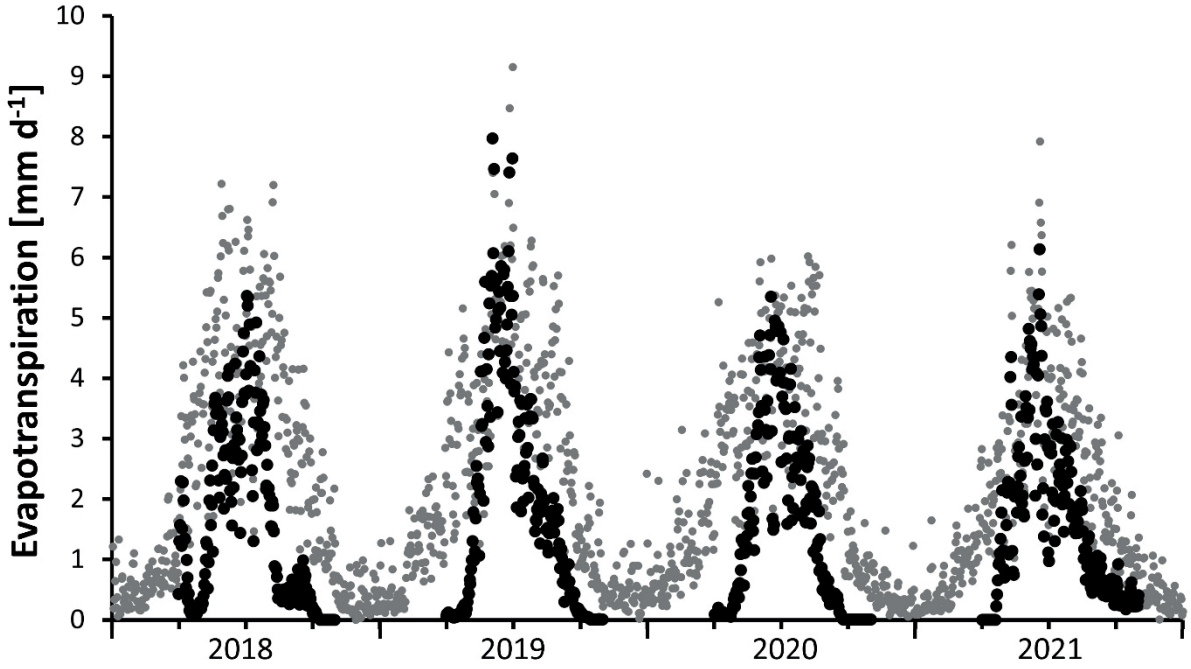

Fig. 4. ET_o (grey dots) from 2018 through 2021 and ET_c of hemp (black dots) during the growing seasons of 2018, 2019, 2020, and 2021. X-axis: Years divided by quartal.

Table 3. Water consumption [mm] by hemp, wheat, and forests over the growing seasons (1st Apr until 31st Oct) 2018, 2019, 2020, and 2021 and precipitation [mm] during the hydrological years (1st Nov of the preceding year until 31st Oct of the given year) and the growing season

Year	Hemp	Wheat	Broad leaf forest	Needle forest	Precipitation during hydrological year	Precipitation during growing season
2018	323	391	638	695	475	248
2019	407	454	654	666	461	291
2020	312	327	567	599	470	284
2021	332	376	508	455	556	397

after the harvest were below 0.1 like during the initial stage. Only DOY 261 of 2018 and DOY 253 of 2021 showed higher K_c values, which corresponds to the comparatively high ET_a on those two days (cf. first paragraph of the result section).

The NDVI of hemp, wheat, broad leaf forest, and needle forest (Fig. 6) coincided with the course of ET_a over the growing seasons. Hemp started out with low NDVIs of below 0.15 until end of April, which matched with the time during which hemp germinated and saplings became visible. During May, the NDVI increased steeply, which reflected that hemp closed its canopy and covered the soil. June, when hemp grew rapidly, and July were characterized by a high NDVI of 0.6 and above. In August, the NDVI fell steeply, as hemp was harvested.

Also for wheat, the development stages were well reflected by the NDVI. While hemp continues to grow until its harvest and therefore maintained its high NDVI until harvest time, wheat ceases to grow and turns yellow when the seed grains ripe. Accordingly, its NDVI dropped sharply at the end of June/beginning of July (around DOY 180), which is ahead of harvest. Only during 2018, the NDVI of wheat dropped already during the beginning of June. While the NDVI of wheat reached values of 0.5 as a maximum around DOY 150 during the growing seasons, it only reached 0.4 during that time of the growing season of 2019.

The courses of the NDVIs of broad leaf forest on the one side and needle forest on the other side followed similar courses during all five growing seasons (Fig. 6).

Discussion

Lisson & Mendham (1998) reported a water consumption of hemp of 359 mm and a stem yield of 10 t ha^{-1} from a field trial in NW Tasmania under rainfed conditions with rainfalls of below 300 mm during the growing season; thus being sim-

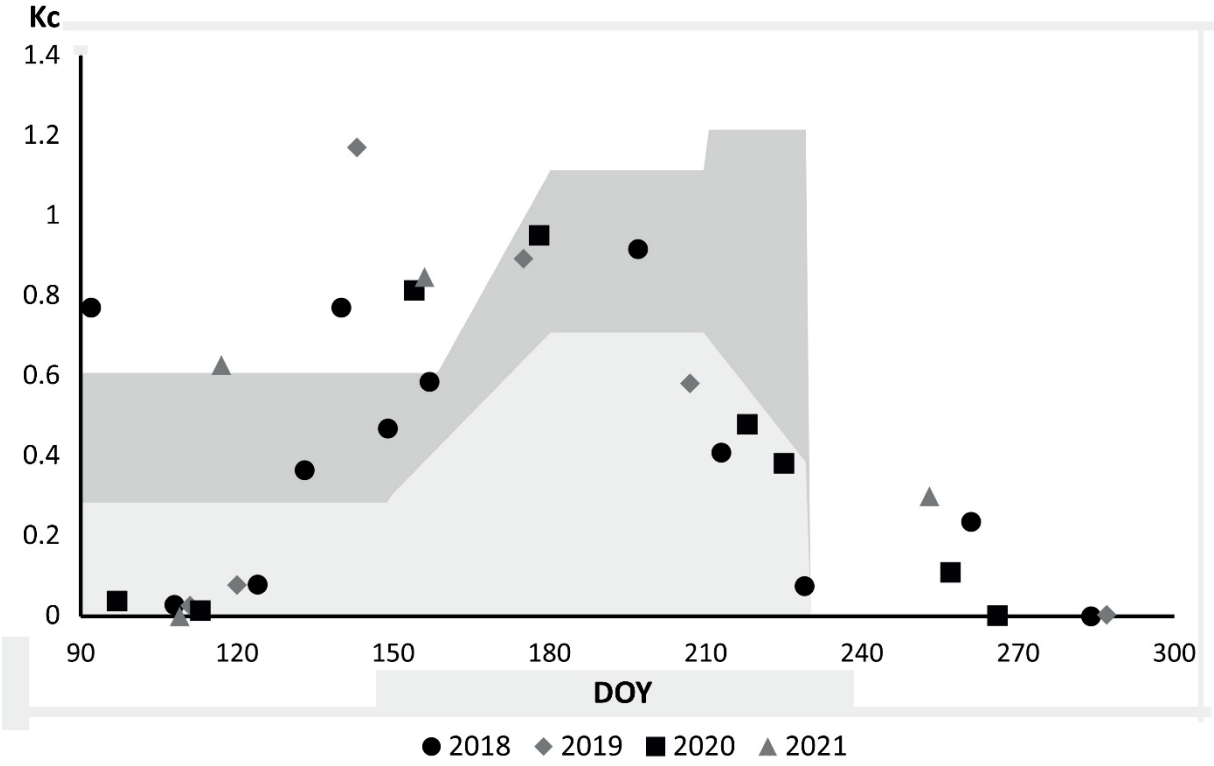

Fig. 5. Kc values calculated from ETo and ETa from the single satellite images during the growing seasons 2018–2021 (symbolized as dots) and range of Kc values from the literature (Thevs & Allen, 2022; Noghabi et al., 2021; García-Tejero et al., 2014; Consentino et al., 2013) symbolized by the grey area. DOY refers to the nth year of each year.

ilar to the numbers in this study. In both studies, the water consumption during the growing season exceeded the precipitation during the growing season. Obviously, hemp was able to use soil moisture that had been accumulated from precipitation before the growing season. The results of this study fall into the range of the results by Consentino et al. (2013), who found that hemp needed 250 mm to 450 mm water and achieved stem yields between 2.3 t ha^{-1} and 14.7 t ha^{-1} depending on the hemp cultivar under a semi-arid climate in Southern Italy.

The water consumption of winter wheat as listed in Table 3 revolves around the water consumption of 424 mm which Li et al. (2008) found for Northern China through the SEBAL approach that is similar to the remote sensing based method applied in this study. The NDIVs of wheat in this study are in the same range as those presented by Qu et al. (2021) also from North China, where winter wheat is sown and harvested at similar times as in NE Germany. For Eastern Germany, Knoblauch (2009) presented an average daily water consumption of 3.9 mm to 4.3 mm for winter wheat during its main growing period. These values correspond to the ET_a values shown in Figure 3 in this study.

Long-term lysimeter trials near Eberswalde, which is approximately 100 km south of the study area, revealed annual water consumptions of 491 mm for a 135-year-old beech (*Fagus sylvatica*) stand. 50- and 84-year-old pine (*Pinus sylvatica*) stands consumed 602 mm and 542 mm per year, respectively (Müller, 2009). The water consumption of broad leaf forest in this study (Table 3), which was between 508 mm and 654 mm exceeded those lysimeter results, while the water consumption of the needle forest as found by this study is in the range of the results from the lysimeter trial.

The data points of the K_c values during the first 30 days of the growing season, as shown in Figure 5, were clearly below the range of K_c values for the initial development as given by the literature. This difference can be explained, as the trials that revealed K_c values were at least partly irrigated so that more water was available to evaporate from the soil surface compared to this study. The two data points that showed a much higher K_c ini value than the literature had been recorded shortly after rain fall events so that the results reflected the evaporation from a then wet soil.

The K_c values between DOY 165 and 200 correspond to the $K_{c\,mid}$ values as given by the literature. Before that, from DOY 135 part of the K_c values of this study are higher than the K_c values from the literature, which is due to the very long initial development stage stated by the literature. The hemp studied here reached canopy closure earlier so that its development stage also started earlier than anticipated by the literature. In addition, the late development stage in this study is earlier than in the literature, because the kc values stem from trials from warmer climates and a therefore longer growing season than in this study area.

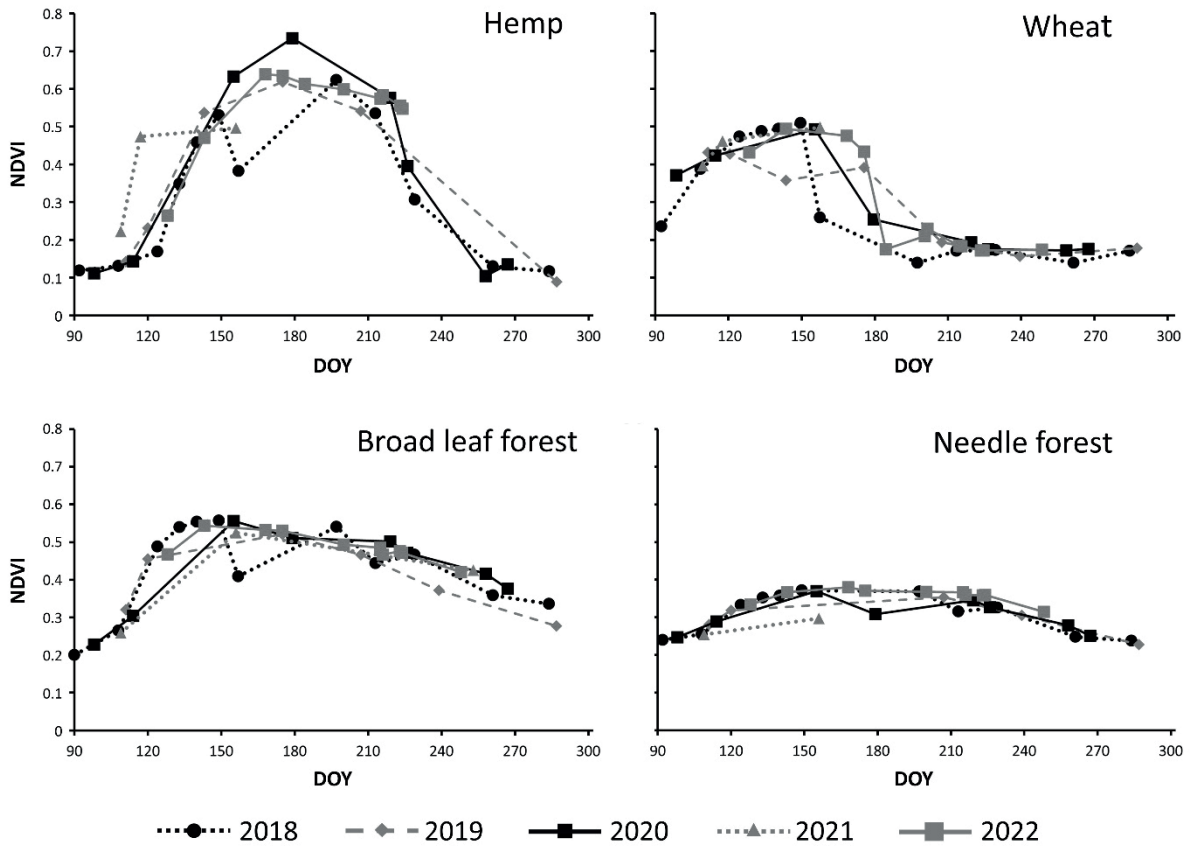

Fig. 6. NDVI for hemp, wheat, broad leaf forests, and needle forests over the growing seasons 2018–2022. DOY refers to the n^{th} year of each year.

The courses of NDVI and ET_a over the five growing seasons were similar for the four crops and vegetations that were studied here. The only exception is wheat, whose NDVI in 2018 already drops in early June instead of late June/early July as in the other years. This can be explained by the extraordinary heat and drought during summer 2018 so that wheat started its senescence earlier and also was harvested earlier. During the following year, 2019, wheat's NDVI reached a lower maximum value than during the other growing seasons, which reflects that the soil moisture has not been replenished after the dry year 2018 so that wheat suffered water stress to some degree. The water consumption of the broad leaf and needle forest decreased each growing season, as shown in Table 3, which reflects that the precipitation was not able to replenish the soil moisture after the during the dry years 2018–2020. Even the substantially higher precipitation during 2021 was not able to replenish the soil moisture and drive the water consumption back to previous levels.

In this study, the S-SEBI approach was chosen to supplement the Penman-Monteith approach rather than assessing daily ET_a by synthetic daily LST images that were created through a fusion of Landsat and MODIS LST layers. The creation of such daily Landsat LSTs was done by Weng et al. (2014), Hazaymeh & Hassan (2015), Zhao et al. (2020), and Salehi et al. (2021).

The study area of NE-Germany faces partial cloud cover during many days of the vegetation period, even during the very dry years that are covered by this study. The Landsat images, which cover the hemp and other field plots represent clear sky and sunny conditions, which result in higher ET_a and ET_c than under cloudy conditions. Therefore, synthetic LST layers, which eventually are based on those Landsat pixels, may cause a bias towards sunny conditions. The calculation of the Landsat ET_a hinges on the so-called cold and hot pixels, which have to be selected manually, because cloud cover, changing water levels, or grazing may render such pixels wrong so that those pixels have to be excluded from further processing. Daily synthetic layers may overlook such errors.

Conclusion

Industrial hemp has the potential to serve as an adaptation to increasingly dry and hot weather conditions, which is already impacting agriculture in several regions of Germany, such as the northeastern part of the country. Hemp develops a deeper root system than most of the other crops that are grown in the region and therefore is able to exploit a larger soil volume or deeper groundwater layers for its water supply. Yet, hemp did not extract more water from the soil than the total precipitation of the given hydrological years so that growing hemp does not constitute an over-exploitation of water. Instead, hemp is able to tap soil moisture that has infiltrated into the soil during autumn and winter. This makes hemp a crop well suited for an adaptation to a drier, hotter, and more variable climate.

Furthermore, the deep root system of hemp increases the organic matter content of the soil, since it adds more root biomass as a feedstock for organic matter into the soil than other crops. Therefore, growing hemp also contributes to increase soil fertility and possibly to carbon sequestration.

Finally, hemp provides fibers and other raw materials that are urgently needed in the course of decarbonization of the economy, which in essence means a shift from oil or gas as a carbon source to biomass as a carbon source for material use.

Conflicts of interest

The authors declare that they do not have any conflicts of interest.

References

Allen, R.G., L.S. Pereira, D. Raes, M. Smith, 1998: Crop evapotranspiration – Guidelines for computing crop water requirements. FAO Irrigation and drainage paper 56. Rome: FAO.

Allen, R.G., M. Tasumi, A. Morse, R. Trezza, 2005: A Landsat-based energy balance and evapotranspiration model in Western US water rights regulation and planning. Irrigation and Drainage Systems **19**, 251–268, DOI: 10.1007/s10795-005-5187-z.

Amaducci, S., H.J. Gusovius, 2010: Hemp-cultivation, extraction and processing. In Müssig, J. (Ed.). Industrial Applications of Natural Fibres: Structure, Properties and Technical Applications (pp. 109–134). West Sussex: John Wiley Sons Ltd.

Amt für Statistik Berlin-Brandenburg, 2019: Besondere Ernte- und Qualitätsermittlung im Land Brandenburg 2018. Potsdam: Landesamt für Statistik..

Bastiaanssen, W.G.M., 1995: Regionalization of surface flux densities and moisture indicators in composite terrain. Ph.D. Thesis. Wageningen: Wageningen University.

Bastiaanssen, W.G.M., M. Menenti, R.A. Feddes, A.A.M. Holtslag, 1998: A remote sensing surface energy balance algorithm for land (SEBAL). 1. Formulation. Journal of Hydrology **212–213**, 198–212, DOI: 10.1016/S0022-1694(98)00253-4.

Bastiaanssen, W.G.M., D.J. Molden, I.W. Makin, 2000: Remote sensing for irrigated agriculture: examples from research and possible applications Agricultural Water Management **46**, 137–155, DOI: 10.1016/S0378-3774(00)00080-9.

Bastiaanssen, W.G.M., M. Ahmad, C.M. Yuan, 2002: Satellite surveillance of evaporative depletion across the Indus Basin. Water Resources Research **38**, 1273–1282, DOI: 10.1029/2001WR000386.

Bastiaanssen, W.G.M., E.J.M. Noordman, H. Pelgrum, G. Davids, B.P. Thoreson, R.G. Allen, 2005: SEBAL Model with remotely sensed data to improve water resouces management under actual field conditions. Journal of Irrigation and Drainage Engineering **131** (1), 85–93, DOI: 10.1061/(ASCE)0733-9437(2005)131:1(85).

Cammalleri, C., G. Ciraolo, G. La Loggia, A. Maltese, 2012: Daily evapotranspiration assessment by means of residual surface energy balance modeling: A critical analysis under

a wide range of water availability. Journal of Hydrology **452-453**, 119-129, DOI: 10.1016/j.jhydrol.2012.05.042.

Consentino, S.L., E. Riggi, G. Testa, D. Scordia, V. Copani, 2013: Evaluation of European developed fibre hemp genotypes (*Cannabis sativa* L.) in semi-arid Mediterranean environment. Industrial Crops and Products **50**, 312-324, DOI: 10.1016/j.indcrop.2013.07.059.

DWD, 2022: Climate Data Center. URL: https://opendata.dwd.de/climate_environment/CDC/observations_germany/climate/daily/weather_phenomena/historical/, Access: 10 Dec 2022.

García-Tejero, I.F., V.H. Durán-Zuazo, R. Pérez-Álvarez, A. Hernández, S. Casano, M. Morón, J.L. Muriel-Fernández, 2014: Impact of Plant Density and Irrigation on Yield of Hemp (Cannabis sativa L.) in a Mediterranean Semi-arid Environment. Journal of Agricultural Science and Technology **16**, 887-895.

Gowda, P.H., J.L. Chavez, P.D. Colaizzi, S.R. Evett, T.A. Howell, J.A. Tolk, 2008: ET mapping for agricultural water management: present status and challenges. Irrigation Science **26**, 223-237, DOI: 10.1007/s00271-007-0088-6.

Gowda, P.H., J.L. Chavez, P.D. Colaizzi, S.R. Evett, T.A. Howell, J.A. Tolk, 2007: Remote sensing based energy balance algorithms for mapping ET: current status and future challenges. American Society of Agricultural and Biological Engineers **50**, 1639-1644, DOI: 10.13031/2013.23964.

Hari, V., O. Rakovec, Y. Markonis, M. Hanel, R. Kumar, 2020: Increased future occurrences of the exceptional 2018–2019 Central European drought under global warming. Scientific Reports **10**, 1–10, DOI: 10.1038/s41598-020-68872-9.

Hazaymeh, K., Q.K. Hassan, 2015: Fusion of MODIS and Landsat-8 Surface Temperature Images: A New Approach. PLOS ONE **10**, e0117755, DOI: 10.1371/journal.pone.0117755.

Hochmuth, H., N. Thevs, P. He, 2015: Water allocation and water consumption of irrigation agriculture and natural vegetation in the Heihe River watershed, NW China. Environmental Earth Sciences **73**, 5269–5279, DOI: 10.1007/s12665-014-3773-9.

Ingrao, C., J. Bacenetti, A. Bezama, V. Blok, P. Goglio, E.G. Koukios, M. Lindner, T. Nemecek, V. Siracusa, A. Zabaniotou, D. Huisingh, 2018: The potential roles of bio-economy in the transition to equitable, sustainable, post fossil-carbon societies: Findings from this virtual special issue. Journal of Cleaner Production **204**, 471–488, DOI: 10.1016/j.jclepro.2018.09.068.

Knoblauch, S., 2009: Wasserhaushaltsgrößen von Kulturpflanzen unter Feldbedingungen. URL: https://www.landwirtschaft.sachsen.de/download/Beregnung_3_Koblauch_wasserhaushaltsgroessen.pdf, Access: 15 Jan 2023.

Kustas, W.P., J.M. Norman, 1996: Use of remote sensing for evapotranspiration monitoring over land surfaces. Hydrological Sciences Journal **41**, 495-516, DOI: 10.1080/02626669609491522.

Li, H., L. Zheng, Y. Lei, C. Li, Z. Liu, S. Zhang, 2008: Estimation of water consumption and crop water productivity of winter wheat in North China Plain using remote sensing technology. Agricultural Water Management **95**, 1271–1278, DOI: 10.1016/j.agwat.2008.05.003.

Liang, S.L., 2000: Narrowband to broadband conversions of land surface albedo I Algorithms. Remote Sensing of Environment **76**, 213-238, DOI: 10.1016/S0034-4257(00)00205-4.

Lisson, S., N. Mendham, 1998: Response of fiber hemp (Cannabis sativa L.) to varying irrigation regimes. Journal of the International Hemp Association 5, 9–15.

Moscariello, C., S. Matassa, G. Esposito, S. Papirio, 2021: From residue to resource: The multifaceted environmental and bioeconomy potential of industrial hemp (Cannabis sativa L.). Resources, Conservation and Recycling **175**, 105064, DOI: 10.1016/j.resconrec.2021.105864.

Müller, J., 2009: Forestry and water budget of the lowlands in northeast Germany – consequences for the choice of tree species and for forest management. Journal of Water and Land Development **13a**, 133–148, DOI: 10.2478/v10025-010-0024-7.

Naumann, G., C. Cammalleri, L. Mentaschi, L. Feyen, 2021: Increased economic drought impacts in Europe with anthropogenic warming. Nature Climate Change **11**, 485–491, DOI: 10.1038/s41558-021-01044-3.

Noghabi, S.G., A. Shahidi, H. Homami, 2021: Estimation of Water Requirement and Crop Coefficient for Hemp at Different Growth Stages in Birjand Plain. Journal of Water Research in Agriculture, DOI: 10.22092/jwra.2021.122794.

Qu, C., P. Li, C. Zhang, 2021: A spectral index for winter wheat mapping using multi-temporal Landsat NDVI data of key growth stages. ISPRS Journal of Photogrammetry and Remote Sensing **175**, 431–447, DOI: 10.1016/j.isprsjprs.2021.03.015.

Rakovec, O., L. Samaniego, V. Hari, Y. Markonis, V. Moravec, S. Thober, M. Hanel, R. Kumar, 2022: The 2018–2020 multi-year drought sets a new benchmark in Europe. Earth's Future **10**, e2021EF002394, DOI: 10.1029/2021EF002394.

Roerink, G.J., B. Su, M. Menenti, 2000: S-SEBI A simple remote sensing algorithm to estimate the surface energy balance. Physics and Chemistry of the Earth, Part B: Hydrology, Oceans and Atmosphere **25** (2), 147–157, DOI: 10.1016/S1464-1909(99)00128-8.

Salehi, H., A. Shamsoddini, S.M. Mirlatifi, B. Mirgol, M. Nazari, 2021: Spatial and Temporal Resolution Improvement of Actual Evapotranspiration Maps Using Landsat and MODIS Data Fusion. Frontiers in Environmental Science **9**, 795287, DOI: 10.3389/fenvs.2021.795287.

Senay, G.B., M. Budde, J.P. Verdin, A.M. Melesse, 2007: A Coupled Remote Sensing and Simplified Surface Energy Balance Approach to Estimate Actual Evapotranspiration from Irrigated Fields. Sensors **7**, 979–1000, PMCID: PMC3795485.

Sobrino, J.A., M. Gómez, J.C. Jiménez-Muñoz, A. Olioso, G. Chehbouni, 2005: A simple algorithm to estimate evapotranspiration from DAIS data: Application to the DAISEX cam-

paigns. Journal of Hydrology **315**, 117–125, DOI: 10.1016/j.jhydrol.2005.03.027.

Sobrino, J.A., M. Gómez, J.C. Jiménez-Muñoz, A. Olioso, 2007: Application of a simple algorithm to estimate daily evapotranspiration from NOAA–AVHRR images for the Iberian Peninsula. Remote Sensing of Environment **110**, 139-148, DOI: 10.1016/j.rse.2007.02.017.

Struik, P.C., S. Amaducci, M.J. Bullard, N.C. Stutterheim, G. Venturi, H.T.H. Cromack, 2000: Agronomy of fibre hemp (Cannabis sativa L.) in Europe. Industrial Crops and Products **11**, 107–118, DOI: 10.1016/S0926-6690(99)00048-5.

Su, Z., 2002: The Surface Energy Balance System (SEBS) for estimation of turbulent heat fluxes. Hydrology and Earth System Sciences **6**, 85-99, DOI: 10.5194/hess-6-85-2002.

Thevs, N., K. Ovezmuradov, L.V. Zanjani, S. Zerbe, 2015: Water consumption of agriculture and natural ecosystems at the Amu Darya in Lebap Province, Turkmenistan. Environmental Earth Sciences **73**, 731–741, DOI: 10.1007/s12665-014-3084-1.

Thevs, N., K. Aliev, 2022: Water consumption of industrial hemp (Cannabis sativa L.) from a site in northern Kazakhstan. Central Asian Journal of Water Research **8**, 19-30, DOI: 10.29258/CAJWR/2022-R1.v8-2/19-30.eng.

Thevs, N., S. Nurtazin, V. Beckmann, R. Salmyrzauli, A. Khalil, 2017: Water Consumption of Agriculture and Natural Ecosystems along the Ili River in China and Kazakhstan. Water **9**, 207, DOI: 10.3390/w9030207.

USGS, 2019: Landsat 8 (L8) Data Users Handbook. Department of the Interior, U.S. Geological Survey. LSDS-1574 Version 5.0. Sioux Falls, South Dakota: EROS. URL: https://www.usgs.gov/landsat-missions/landsat-8-data-users-handbook, Access:16-Jan-2023.

Waters, R., R.G. Allen, M. Tasumi, R. Trezza, W.G.W. Bastiaanssen, 2002: SEBAL Surface Energy Balance Algorithms for Land – Idaho Implementation – Advanced Training and Users Manual. University of Idaho, USA.

Weng, Q., P. Fu, F. Gao, 2014: Generating daily land surface temperature at Landsat resolution by fusing Landsat and MODIS data. Remote Sensing of Environment **145**, 55–67, DOI: 10.1016/j.rse.2014.02.003.

Zhao, G., Y. Zhang, J. Tan, C. Li, Y, Ren, 2020: A Data Fusion Modeling Framework for Retrieval of Land Surface Temperature from Landsat-8 and MODIS Data. Sensors **20**, 4337, DOI: 10.3390/s20154337.